Improved Designs for an Electrothermal In-Plane Microactuator

Alex Man Ho Kwan, *Student Member, IEEE*, Sichao Song, *Student Member, IEEE*, Xing Lu, Lei Lu, Ying-Khai Teh, *Student Member, IEEE*, Ying-Fei Teh, Eddie Wing Cheung Chong, Yan Gao, William Hau, Fan Zeng, Man Wong, *Senior Member, IEEE*, Chunmei Huang, Akira Taniyama, Yoshihide Makino, So Nishino, Toshiyuki Tsuchiya, *Member, IEEE*, and Osamu Tabata, *Senior Member, IEEE*

***Abstract*—Reported presently are two design approaches to improve the performance of an electrothermal in-plane microactuator with "chevron" beams. One incorporates beams with uniform cross sections but nonuniform lengths or tilt angles to accommodate the thermally induced expansion of the "shuttle"; the other incorporates beams with nonuniform cross sections to widen the high-temperature "expansion" zones. It is derived analytically, verified using finite-element simulations, and tested by microfabricating actuators occupying a constrained device area that the incorporation of one or the other proposed features leads to an improved performance figure-of-merit, defined to be the product of the actuation displacement and force. An increase in the figure-of-merit by up to 65% per beam has been measured. [2011-0186]**

***Index Terms*—Electrothermal microactuators, in-plane chevron microactuators, microelectromechanical systems (MEMS), optimization.**

I. Introduction

PIEZOELECTRIC [1], magnetostatic [2], electrostatic [3], [4], and electrothermal [5]–[8] are popular drive mechanisms implemented in microactuators. Piezoelectric material is typically not process compatible with silicon. Electrothermal actuators, unlike magnetostatic and electrostatic actuators, can generate larger force and displacement—although they are relatively slower.

Unlike an asymmetric bent-beam electrothermal actuator [5], [6] employing Joule's heating, a "chevron" electrothermal actuator (see Fig. 1) provides not only a scalable force through the inclusion of multiple chevron "actuation" beams but also a displacement that is confined ideally in one dimension [8]. Chevron actuators have been incorporated in a number of microelectromechanical systems, such as tunable diffraction gratings [9], gear motors [10], [11], and microtweezers [12]. However, the performance of a conventional chevron actuator is limited by a high-temperature "expansion" zone that is narrowly confined near the center of a given chevron beam (hereafter simply designated as "beam") and degraded by the thermal expansion of a relatively long "shuttle" that connects the apexes of the beams. Reported presently are two design approaches to improve the performance of such an actuator. One incorporates beams with nonuniform lengths L and tilt angles θ to accommodate the thermally induced expansion of the shuttle; the other incorporates beams with nonuniform cross sections to widen the expansion zones.

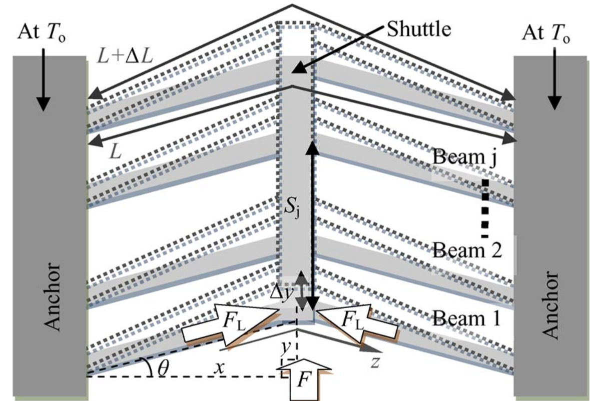

Fig. 1. Schematic drawing of a conventional chevron actuator, showing the deformation of the beams induced by Joule's heating.

Consider again the actuator shown in Fig. 1. Each beam is mechanically fixed at its two ends to the "anchors" that not only provide rigid mechanical support but also function as heat sinks and electrical contacts. When a voltage V_a is applied across a beam, an electric current I is induced, and heat is generated because of the finite resistivity ρ of the beam. The apex at the center of the beam is raised to a temperature ΔT_M above that (T_o) of the anchors and moves "up" by Δy (the actuation displacement) as a result of the thermally induced expansion ΔL of the beam. The shuttle links the apexes and aggregates the actuation force of the multiple beams, resulting in a total actuation force F (*pulling* in the present case) manifested at its "bottom end."

Although there are other metrics that account for dynamic response such as frequency [13], the performance of an actuator is presently quantified by a figure-of-merit $\eta \equiv \Delta y_o F_o$, where $\Delta y_o \equiv \Delta y|_{F=0}$ is the displacement at zero loading (i.e., the "unloaded" displacement) and $F_o \equiv F|_{\Delta y=0}$ is the actuation force at zero displacement. This η is a suitable metric for

Manuscript received June 20, 2011; revised December 27, 2011; accepted January 16, 2012. Date of publication February 22, 2012; date of current version May 28, 2012. Subject Editor D. Elata.

A. M. H. Kwan, S. Song, X. Lu, L. Lu, Y.-K. Teh, Y.-F. Teh, E. W. C. Chong, Y. Gao, W. Hau, F. Zeng, and M. Wong are with the Department of Electronic and Computer Engineering, The Hong Kong University of Science and Technology, Kowloon, Hong Kong (e-mail: alexmhkwan@ust.hk; e-mail: eemwong@ece.ust.hk).

C. Huang, A. Taniyama, Y. Makino, S. Nishino, T. Tsuchiya, and O. Tabata are with the Department of Microengineering, Graduate School of Engineering, Kyoto University, Kyoto 606-8501, Japan.

Color versions of one or more of the figures in this paper are available online at http://ieeexplore.ieee.org.

Digital Object Identifier 10.1109/JMEMS.2012.2185820

1057-7157/$31.00 © 2012 IEEE

applications requiring both finite displacement and finite force. Naturally, a "better" design is one that leads to a larger η.

II. Design One: Beams With Uniform Cross Sections But Nonuniform Lengths or Tilt Angles

The I-induced heat-generation rate per unit volume G is constant along a beam with a uniform cross section and a constant ρ. Assuming that the removal of the generated heat by radiation and convection is negligible compared to conduction, one obtains a temperature distribution $T(z)$ approximately governed by $G \approx -k(\mathrm{d}^2T(z)/\mathrm{d}z^2)$, a 1-D heat-transfer equation with z and k denoting respectively the distance along the length and the thermal conductivity of the beam. With the heat sinks located at $z = 0$ and $z = L$, and $T(0) = T(L) = T_o$, a "parabolic" temperature distribution can be derived as $T(z) \approx 4\Delta T_M[-(z/L)^2 + z/L] + T_o$. For a beam with a thermal expansion coefficient of α, ΔL at $F = 0$ can be estimated

$$\Delta L = \alpha \int_0^L [T(z) - T_o]\,\mathrm{d}z \approx \frac{2}{3}\alpha L \Delta T_M. \tag{1}$$

Assuming a rigid-body beam [7] but ignoring the elastic restoring force at the apex where the beam joins the shuttle, one derives $\Delta L \approx 2\theta\Delta y_o$ for a small tilt angle θ such that $\sin\theta \approx \theta$. Combining this with (1), one obtains

$$\Delta y_o \approx \frac{\Delta L}{2\theta} \approx \frac{\alpha\Delta T_M}{3}\left(\frac{L}{\theta}\right). \tag{2}$$

Collected inside the bracket on the right-hand side of (2) are the terms representing the geometric parameters of the beam.

The shuttle is also heated to a temperature approaching $\Delta T_M + T_o$ by the heat generated at the apexes of the beams; hence, it thermally expands. For a Beam j with an apex separated from that of the "reference" Beam 1 by S_j, an additional displacement of $\Delta S_j \approx S_j\alpha\Delta T_M$ needs to be added to the displacement of its apex to accommodate the thermally expanded shuttle. Any $\Delta S_j \neq 0$, if not properly accounted for, reduces the overall η of the actuator. The more the number of beams, the longer is the shuttle and the greater the potential reduction in η.

To fully accommodate the effects of ΔS_j on η, one needs to adjust the length L_j and the tilt angle θ_j of Beam j such that (2) is satisfied for each beam

$$\Delta y_{\mathrm{oj}} \approx \frac{\alpha\Delta T_M}{3}\left(\frac{L_j}{\theta_j}\right). \tag{3}$$

Since $\Delta y_{\mathrm{oj}} = \Delta y_{o1} + \Delta S_j \approx \Delta y_{o1} + S_j\alpha\Delta T_M$, one obtains using (3)

$$\frac{L_j}{\theta_j} \approx \frac{L_1}{\theta_1} + 3S_j \tag{4}$$

where Δy_{oj} and Δy_{o1} are the respective unloaded displacement of Beams j and 1; L_1 and θ_1 are the respective length and tilt angle of Beam 1. Note that these design constraints are independent of V_a, the beam temperature, or the material constants.

TABLE I
Geometric Parameters of the Beams for a Staircase Actuator

Group	L	θ	Number of Beams
1	420μm	2.60°	7
2	400μm	2.73°	9
3	380μm	2.86°	10
4	360μm	3.01°	11
5	340μm	3.18°	12

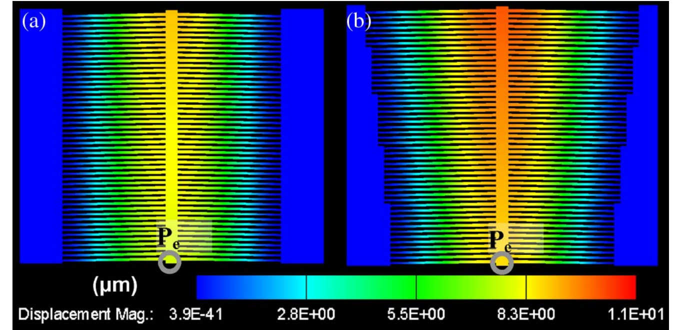

Fig. 2. Layouts and the simulated Δy at $V_a = 4.8$ V of (a) a conventional and (b) a staircase actuator with L and θ listed in Table I. The color contour reflects the magnitude of Δy. Note the nonuniform Δy in (b), resulting from the thermally induced expansion of the shuttle.

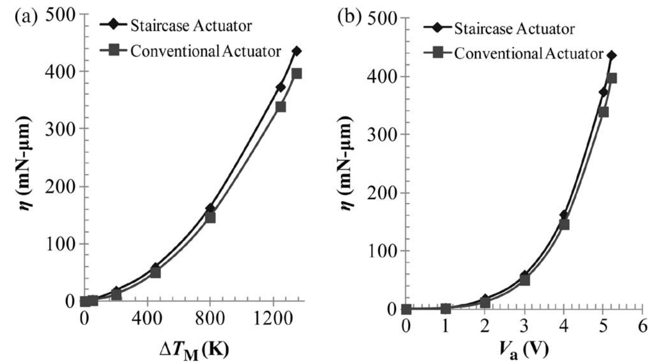

Fig. 3. Simulated dependence of η on (a) ΔT_M and (b) V_a for both the conventional and the staircase chevron actuators. The L and θ of the staircase actuator are listed in Table I.

Since the beams within a short stretch of the shuttle exhibit a small variation in ΔS_j, they can be grouped to share the same L and θ. Given in Table I is an example of a "staircase" actuator with 49 beams divided into five groups. The respective layouts of a conventional and a staircase actuator are shown in Fig. 2(a) and (b). The respective "fixed" L and θ for the former are 340 μm and 3.18°.

Simulations were performed with F and Δy measured at the "point-of-engagement" P_e (see Fig. 2) of the shuttle. The simulated dependence of η on ΔT_M (up to a value just below the melting point of silicon at ~1687 K) and the corresponding V_a are respectively shown in Fig. 3(a) and (b). When compared at a given ΔT_M or V_a, the simulated η of a staircase actuator is ~10% larger than that of the conventional design.

III. Design Two: Beams With Nonuniform Cross Sections for Improved Temperature Distribution

The parabolic temperature distribution induced by the Joule's heating of a beam with a uniform width exhibits a relatively sharp peak at the apex of the beam, leaving a significant portion of the beam at a lower temperature that contributes little to the "actuation process." This "waste" could be recovered if the temperature $T(z)$ along a beam were distributed more like a rectangular "box" than a parabola such that the high-temperature zone would extend over a longer stretch of the beam. Proposed in (5) is an analytical model approximating a box profile. In principle, such a distribution can be constructed as the product of two generic step functions. In the present case, the step function chosen is modeled after the familiar Fermi–Dirac distribution function, with β parameterizing the "steepness" of the transitions

$$T(z) = \Delta T_M \left(\frac{1+e^{-\frac{L}{2\beta}}}{1-e^{-\frac{L}{2\beta}}}\right)^2 \times \left[\frac{2\left(1+e^{-\frac{L}{\beta}}\right)}{\left(1+e^{-\frac{z}{\beta}}\right)\left(1+e^{\frac{z-L}{\beta}}\right)} - 1\right] + T_o. \quad (5)$$

Assuming that heat removal is dominated by conduction, one derives the steady-state heat-generation rate $G(z) \approx -k(\mathrm{d}^2T(z)/\mathrm{d}z^2)$ using the $T(z)$ given in (5). Since this is due to Joule's heating, the current density $J(z)$ is given by $J(z) = \sqrt{G(z)/\rho}$

$$J(z) \approx \frac{1}{\beta}\sqrt{\frac{2k\Delta T_M}{\rho}\left(1+e^{-\frac{L}{\beta}}\right)}\left(\frac{1+e^{-\frac{L}{2\beta}}}{1-e^{-\frac{L}{2\beta}}}\right) \times \sqrt{\frac{\left(e^{-\frac{z}{\beta}}+e^{\frac{z-L}{\beta}}\right)\left(1-e^{-\frac{z}{\beta}}\right)\left(1-e^{\frac{z-L}{\beta}}\right)+8e^{-\frac{L}{\beta}}}{\left(1+e^{-\frac{z}{\beta}}\right)^3\left(1+e^{\frac{z-L}{\beta}}\right)^3}}. \quad (6)$$

The resulting $T(z)$ and $J(z)$ are plotted in Fig. 4. An ideally flat temperature profile implies a vanishingly small $J(z)$ such that $G(z)$ approaches zero and Joule's heating is nearly shut down. This is the case when β is small and the temperature gradient is steep, as shown in Fig. 4(a). In practice, I is finite, and $J(z)$ cannot be arbitrarily small; hence, the transition cannot be arbitrarily sharp. This more realistic case is shown in Fig. 4(b).

Since $I = tW(z)J(z)$, where t and $W(z)$ are the respective thickness and the variable width of a beam, $W(z)$ can be determined once $J(z)$ is known

$$W(z) = \frac{I\beta}{t}\sqrt{\frac{\rho}{2k\Delta T_M\left(1+e^{-\frac{L}{\beta}}\right)}}\left(\frac{1-e^{-\frac{L}{2\beta}}}{1+e^{-\frac{L}{2\beta}}}\right) \times \sqrt{\frac{\left(1+e^{-\frac{z}{\beta}}\right)^3\left(1+e^{\frac{z-L}{\beta}}\right)^3}{\left(e^{-\frac{z}{\beta}}+e^{\frac{z-L}{\beta}}\right)\left(1-e^{-\frac{z}{\beta}}\right)\left(1-e^{\frac{z-L}{\beta}}\right)+8e^{-\frac{L}{\beta}}}}. \quad (7)$$

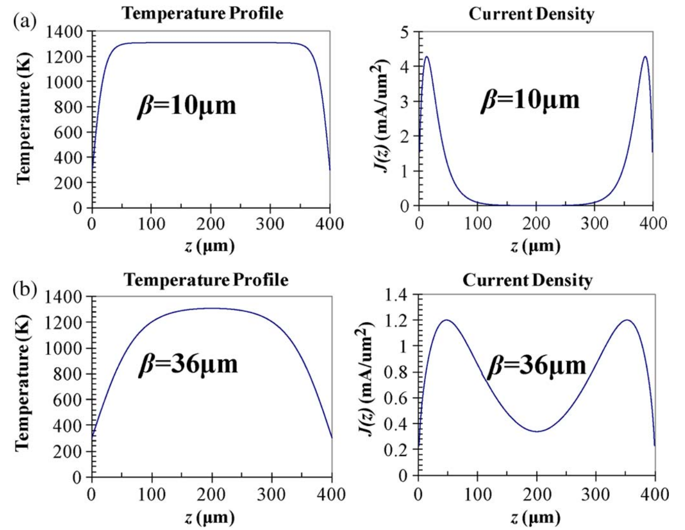

Fig. 4. (a) $T(z)$ and $J(z)$ with sharp ($\beta = 10\ \mu$m and $L = 400\ \mu$m) transition. Note that J is almost zero near the center for the beam. (b) More realistic $T(z)$ and $J(z)$, with $\beta = 36\ \mu$m and $L = 400\ \mu$m.

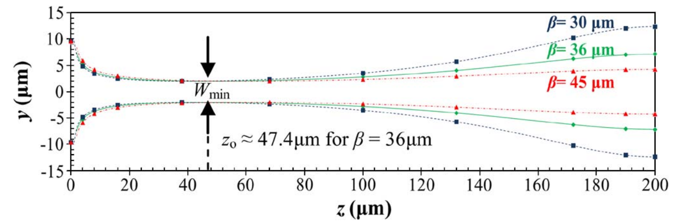

Fig. 5. Variation of $W(z)$ along a half beam for $\beta = 30$, 36, and 45 μm. The beam is anchored at $z = 0\ \mu$m and connects to the shuttle at $z = 200\ \mu$m. The positions indicated by the dots are used to construct a polygonal representation of the beam used for layout and in the simulations.

The "neck" of the beam, defined to be the part of the beam with the narrowest width $W_{\min}$, is located at z_o from the anchor

$$z_o = \beta \ln\left\{\frac{1}{2}\left[(2-\sqrt{3})\left(1+e^{\frac{L}{\beta}}\right) - \sqrt{(7-4\sqrt{3})\left(1+e^{\frac{2L}{\beta}}\right) - 2(4\sqrt{3}-5)e^{\frac{L}{\beta}}}\right]\right\}. \quad (8)$$

The choice of $W_{\min}$ is constrained by both the mechanical strength required of the beam and the resolution of the photolithography. It cannot be made arbitrarily small and is chosen to be 4 μm in the present implementation. The half-beam profiles for three different values of β are shown in Fig. 5. For ease of layout, the analytical profile of (7) is approximated using a polygonal profile, with the vertices defined by the points indicated in the figure.

The $T(z)$'s in the beams with uniform and nonuniform widths were simulated and compared in Fig. 6. At the necks near the anchors of a beam with a nonuniform width, both $J(z)$ and $G(z)$ are the highest. In the wider region between the "necks," both $J(z)$ and $G(z)$ are reduced. Consequently, the temperature rise is suppressed, and a flatter $T(z)$ is obtained. Therefore, a larger portion of the beam can be utilized for thermal actuation. Shown in Fig. 7 are the $T(z)$'s of actuators, each containing a pair of beams with uniform or nonuniform

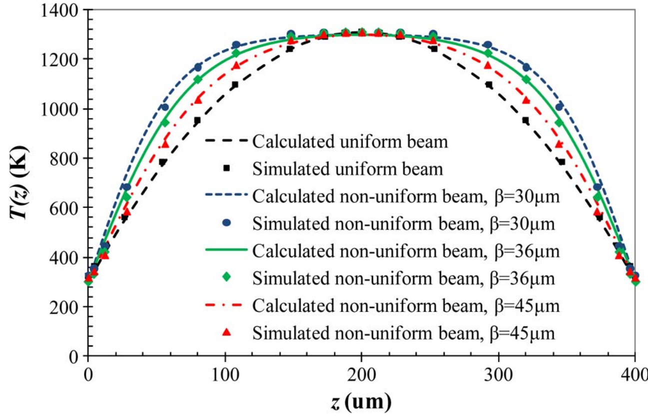

Fig. 6. Dependence of $T(z)$ on z for a modified beam with $\beta = 30$, 36, or 45 μm and biased at a V_a such that $\Delta T_M + T_o$ is 1300 K. The $T(z)$ of a beam with a W is also shown for comparison.

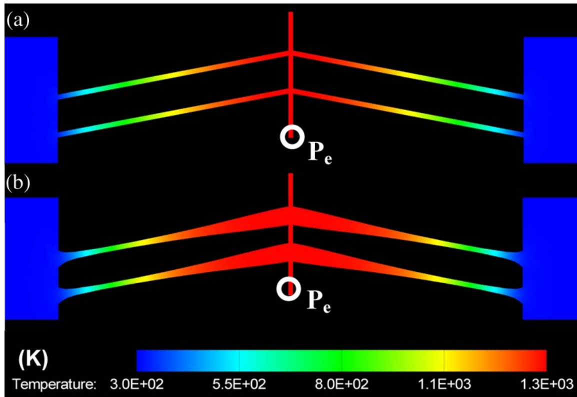

Fig. 7. Simulated $T(z)$ along the beams ($L = 400$ μm) with (a) uniform and (b) nonuniform widths. The width of the uniform beam in (a) is 4 μm, and $\beta = 36$ μm for the nonuniform beam in (b). V_a is biased such that $\Delta T_M + T_o$ is 1300 K.

widths. The beams are separated by 20 μm, with a tilt angle of 10°. Clearly, the "red" high-temperature zones extend over longer stretches [see Fig. 7(b)] of the beams with nonuniform cross sections.

The corresponding ΔL at $F_o = 0$ is estimated using (1)

$$\Delta L \approx \alpha \Delta T_M \left(\frac{1 + e^{-\frac{L}{2\beta}}}{1 - e^{-\frac{L}{2\beta}}} \right)^2 \times \left[4\beta \left(\frac{1 + e^{-\frac{L}{\beta}}}{1 - e^{-\frac{L}{\beta}}} \right) \ln \left(\frac{1 + e^{\frac{L}{\beta}}}{2e^{\frac{L}{2\beta}}} \right) - L \right]. \quad (9)$$

Shown in Fig. 8 is the dependence of ΔL on ΔT_M, for beams with uniform and nonuniform widths. Because of their wider high-temperature zones, the simulated ΔL's for beams with nonuniform widths are 12.3% (for $\beta = 30$ μm) and 8.6% (for $\beta = 36$ μm) larger than that of the corresponding beams with uniform widths. The small deviations between the simulated and the analytically calculated $T(z)$ and ΔL, shown respectively in Figs. 6 and 8, are due to the nonideal polygonal shapes used in the simulations.

The simulated dependences of η on ΔT_M or V_a for a number of designs are compared in Fig. 9. The simulated η is clearly

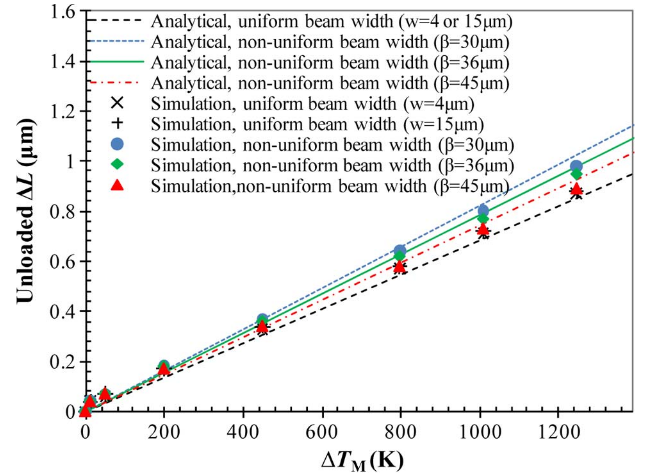

Fig. 8. Dependence of ΔL at $F = 0$ on ΔT_M of various beams ($L = 400$ μm) along the beam length.

larger for beams with nonuniform cross sections. The smaller the β is, the greater the η is at the same ΔT_M or V_a. The trend follows that displayed in Fig. 8, showing the effectiveness of a widened high-temperature expansion zone of a beam with a nonuniform width. Above 1550 K, the η of an actuator with beams of uniform widths saturates because the beams buckle and cannot generate more F even if V_a is further increased [8]. This is also evident in Fig. 9(b). In this situation, the rigid body beam model may not be applicable. Below 1550 K, the η of the actuators with nonuniform beamwidths for $\beta = 30$, 36, and 45 μm are, respectively, 118%, 65%, and 40% larger than that of an actuator with uniform beamwidths of 4 μm.

The η of an actuator can be approximately analyzed by starting with the expression for $F_o \approx 2NF_L \sin\theta \approx 2NF_L\theta$ along the direction of the shuttle, where $F_L \approx (Et\widetilde{W}/L)\Delta L/2$ is the axial force exerted at the shuttle by a half beam shown in Fig. 1. E is the Young's modulus of the beam; $\widetilde{W}$ or W is the respective weighted or the actual width of a beam with nonuniform or uniform widths. Using (2), one calculates $\eta = \Delta y_o F_o \approx (NE/2L)t\widetilde{W}\Delta L^2$. The ratio of η_n of an actuator containing N_n beams with nonuniform widths to η_u of an actuator containing N_u beams with uniform widths is

$$\frac{\eta_n}{\eta_u} \approx \frac{N_n}{N_u} \frac{\widetilde{W}}{W} \left(\frac{\Delta L_n}{\Delta L_u} \right)^2. \quad (10)$$

Therefore, when $N_n = N_u$, both $\Delta L_n > \Delta L_u$ (see Fig. 8) and $\widetilde{W} > W$ contribute to making $\eta_n > \eta_u$.

Compared to the improvement in η, the improvement in Δy_o of the actuators with beams with nonuniform widths over that of an actuator with beams with a uniform $W = 4$ μm is relatively small [see Fig. 10(a)]: ~3.9% (for $\beta = 30$ μm) or ~3.2% (for $\beta = 36$ μm). This is because, in the former case, the widths of the beams near the shuttle are larger, hence also the resulting elastic force against deformation. The improvement in F_o [see Fig. 10(b)], at ~114% (for $\beta = 30$ μm) and ~62% (for $\beta = 36$ μm), contributes more to the improvement in η. If a design calls for a larger Δy_o, then perhaps the inclusion of a lever system to amplify displacement is a possible solution while sacrificing a fraction of F_o.

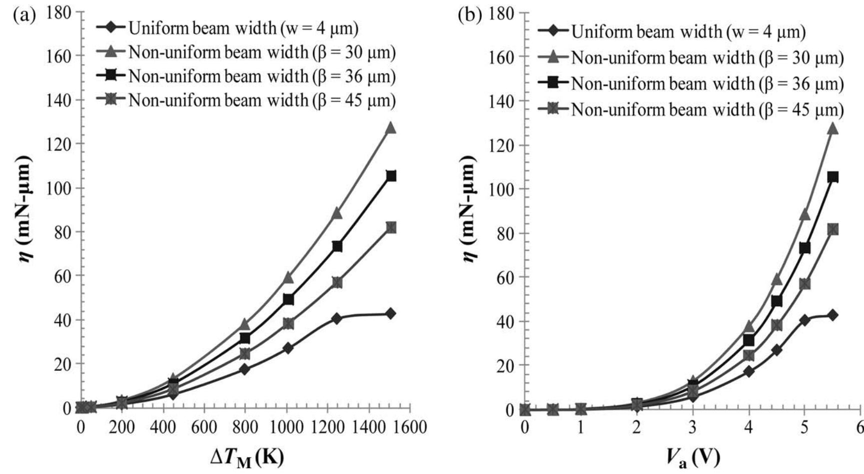

Fig. 9. Dependence of the simulated η on (a) ΔT_M and (b) V_a for chevron actuators of $L = 400\ \mu$m with various β.

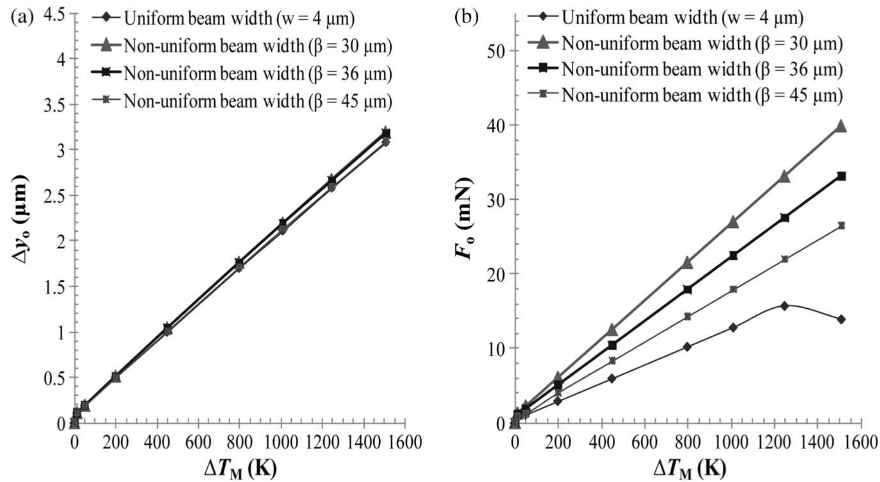

Fig. 10. Dependence of simulated (a) Δy_o and (b) F_o on ΔT_M of chevron actuators of $L = 400\ \mu$m with various β.

IV. Stress Distribution and the Effect of Undercut

Shown in Fig. 11(a)–(c) are the distributions of the von Mises stress in the designs investigated in the present work. It can be noted and shown in Fig. 11(d) and (e) that the stress is mostly concentrated around the lever system rather than at the locations where the beams connect to the shuttle or the anchors. This is consistent with the assumption used in the derivation of (2) that the elastic restoring force at the apex, where the beam joins the shuttle, is small.

An undercut of $\sim$20 μm was created around the periphery of the anchors during the structural release, and its effects on the mechanical boundary condition are simulated. Shown in Fig. 12(c) and (d) are the displacements at the location where the beams are attached to the anchor with an undercut of 20 μm. The displacement of less than 0.25 μm is much smaller than the practical resolution of measurement of the actuators.

V. Fabrication and Measurement Results

A variety of chevron actuators were fabricated on silicon-on-insulator wafers with 15-μm-thick silicon structural layers and 2-μm-thick buried-oxide sacrificial layers. The device layer was heavily doped with $\sim 10^{20}$ cm^{-3} phosphorus. Since this is significantly higher than the intrinsic carrier concentration of $\sim 5 \times 10^{19}$ cm^{-3} near the melting point of silicon, the beams remain "extrinsic" under all practical bias conditions. The structure is formed employing typical photolithography, dry etching, and metal liftoff processes.

The final release was performed in a buffered oxide-etchant solution. The estimated undercut of the buried-oxide sacrificial layer is 16 μm on each side. This is significantly less than the 100-μm side length of an anchor and should not adversely affect the assumption of a rigid mechanical boundary at the anchor.

The specifications of the designs are as follows: $\Delta y_o \geq 10\ \mu$m at P_e and device area $\leq 500 \times 500\ \mu$m^2. For the design of the 49-beam staircase actuator described in Section II, the maximum displacement is about 8 μm, thus requiring the incorporation of a lever structure with a displacement amplification of $\sim$1.3. The levers are visible at the bottom of the pictures shown in Fig. 13(a) and (b).

For the design of an actuator with nonuniform beamwidths, since the overall η is significantly improved as discussed in Section III, fewer beams need to be incorporated, as shown in Fig. 14. With a shorter shuttle resulting from the fewer beams, the detrimental effects of the shuttle expansion can be

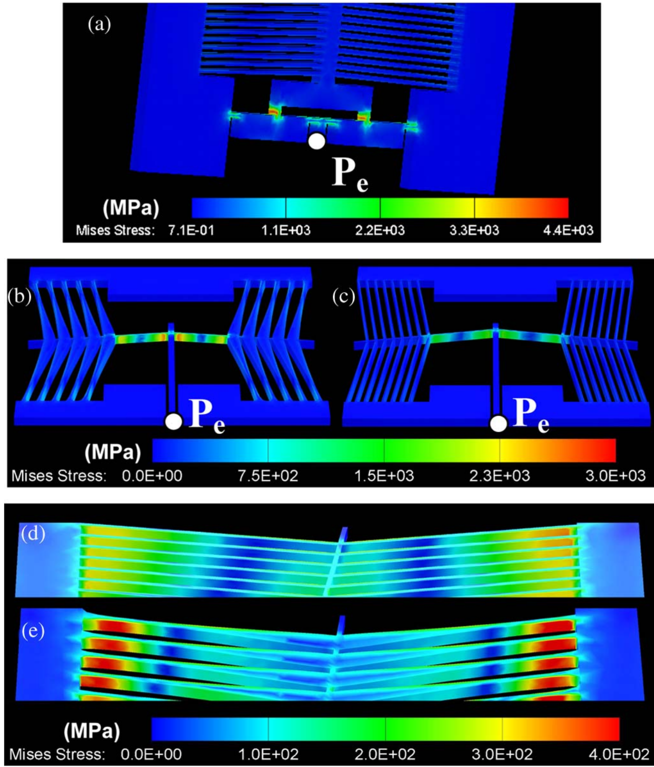

Fig. 11. Simulated von Mises stress of (a) a staircase actuator and a double-chevron actuator with (b) nonuniform ($\beta = 36\ \mu$m) and (c) uniform widths biased at $V_a = 4.8$ V. The stress along the beams of structures (b) and (c) are shown in (d) and (e), respectively.

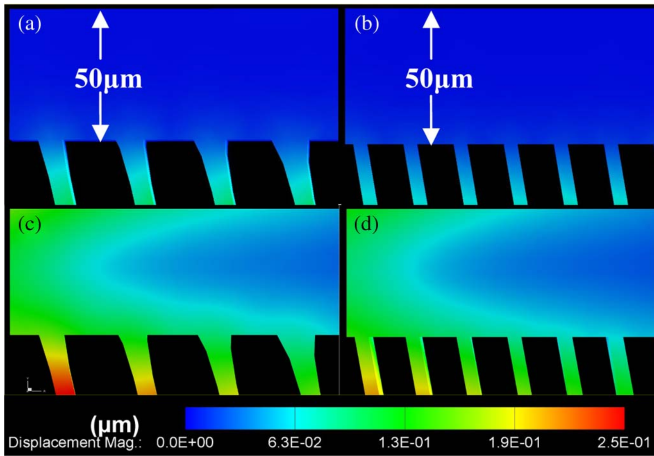

Fig. 12. Displacement of a double-chevron actuator with beams of (a) nonuniform ($\beta = 36\ \mu$m) and (b) uniform widths with zero undercut. (a) and (b) are zoomed to the location where the beams are attached to the anchors as in Fig. 11(b) and (c), respectively. (c) and (d) are the same structure of (a) and (b), respectively, with a 20-μm undercut. All are set at $V_a = 4.8$ V, arranged for the maximum actuation force at zero displacement of P_e.

neglected. The shuttles of the two chevron actuators on each side are connected to a lever. The tilt angles of the shuttles can be adjusted to trade off part of F_o for a larger Δy_o. It can be shown that $\Delta y_o \approx \Delta L/(2\theta_1\theta_2)$ for this "double-chevron" actuator. This type of actuators has been introduced in [14] and [15], and the modeling of this structure has been discussed in [16].

The fabricated double-chevron actuators using beams with uniform widths of 4 μm and nonuniform widths with $\beta =$

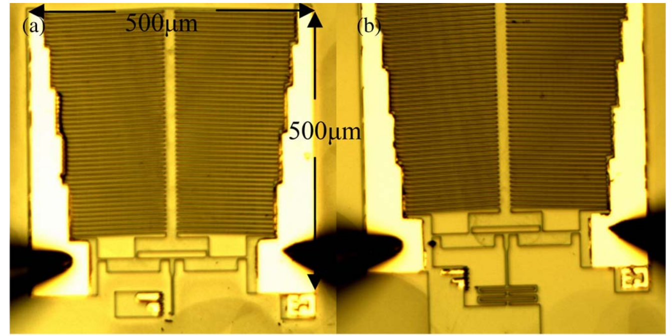

Fig. 13. Fabricated (a) unloaded and (b) spring-loaded staircase actuators, with L and θ specified in Table I.

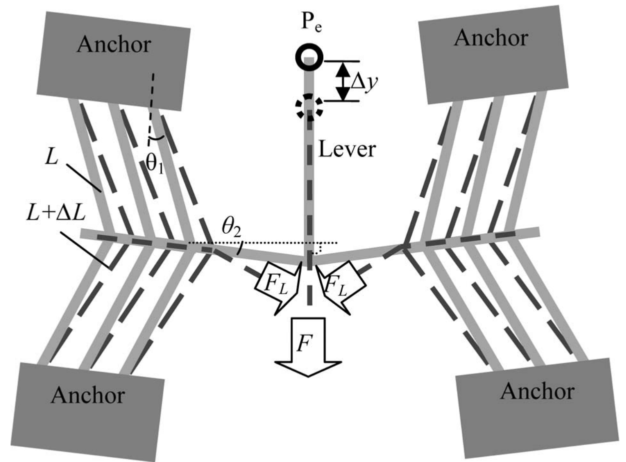

Fig. 14. Schematic drawing of a double-chevron actuator, showing the deformation induced by Joule's heating.

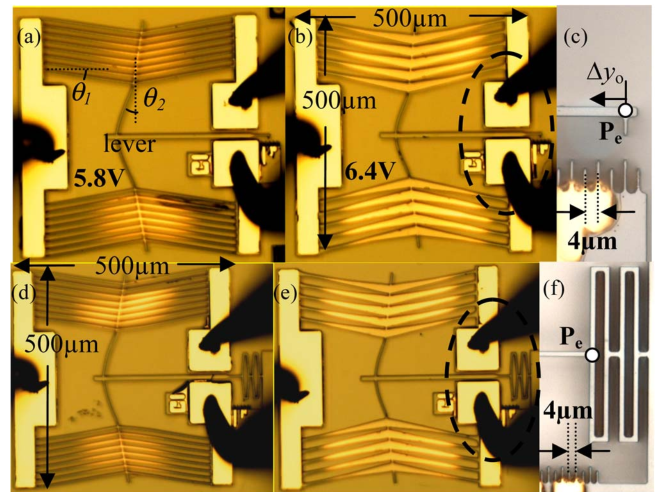

Fig. 15. Fabricated double-chevron actuators with (a) uniform beamwidths of 4 μm and (b) nonuniform beamwidths with $\beta = 36\ \mu$m and $L = 400\ \mu$m. (c) Zoomed view of the dotted circle in (b), showing displacement Δy_o of the needle on the lever read against an integrated scale, with a resolution of 2 μm. Shown in (d) and (e) are the actuators for measuring F using a standard spring. (f) Zoomed view of the dotted circle in (e), showing Δy at P_e read against an integrated scale, with a resolution of 2 μm.

36 μm and $W_{\min} = 4\ \mu$m are shown in Fig. 15. The same tilt angles of $\theta_1 = 10^\circ$ and $\theta_2 = 11.5^\circ$, shuttle length of 80 μm, and beam length of $L = 400\ \mu$m are used for both types of

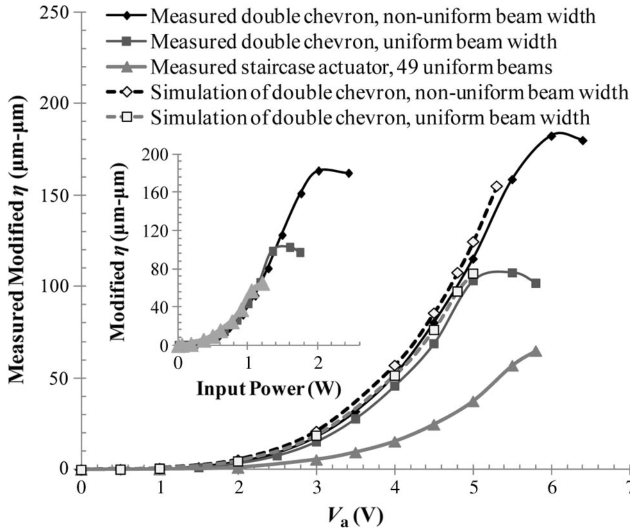

Fig. 16. Measured modified η versus V_a. Shown in the inset is the measured modified η versus input power.

actuators. Levers with an amplification factor $(1/\theta_2 \approx 5)$ are incorporated to realize a Δy_o of $\sim 10\ \mu$m. Consistent with the temperature distribution shown in Fig. 6, a significantly wider "glow" (i.e., high-temperature) zone is indeed verified on the actuator with nonuniform beamwidths.

The Δy_o of the actuators was measured by "sweeping" V_a across the anchors. When the lever actuates, a needle at its end "reads" the displacement against a scale that has been fabricated simultaneously with the device, as shown in Fig. 15(c). To estimate F, their P_e's are attached to a "standard" spring as shown in Figs. 13(b) and 15(d) and (e). The distortion of the springs largely follows Hooke's law such that F is linearly converted to a displacement at P_e, as shown in Fig. 15(f). Since the force is not directly measured, the measured η is represented as a product of the unloaded Δy_o and the displacement of P_e loaded with a spring.

The measured η of various actuators is shown in Fig. 16. At a given V_a, the staircase actuator with 49 beams draws more I than the double-chevron actuator that uses a fewer number of beams. The melting of silicon ultimately bounds the maximum value of η and causes it to "saturate." Prior to saturation, the η at a given V_a of a double-chevron actuator with a uniform beamwidth is about the same as that of the actuator with nonuniform beamwidths. This lack of an improvement in η is apparently inconsistent with the analytical prediction given earlier. This is because there are more beams $(N_u = 16)$ in the actuator with uniform beam cross sections than there are beams $(N_n = 10)$ in the actuator with nonuniform beam cross sections. When this difference is taken into account, it can be deduced that the η of the actuator with nonuniform beamwidth $(\beta = 36\ \mu\text{m})$ is ~65% per beam larger than that of the actuator with a uniform beamwidth of 4 μm. Such measured results of the double-chevron actuators are consistent with the simulation data, with the simulation stopped at the largest V_a before the melting point of silicon. The small discrepancy may include the ignored finite contact resistance between the probe and the metal on the anchor and the linewidth loss due to process variation.

It is apparent that the double-chevron actuator with uniform beamwidths becomes saturated at a lower value of η, compared to that with nonuniform beamwidths. Such early saturation is also consistent with the simulation shown in Figs. 9(a) and (b) and 10(b). This is because the former exhibits a more gradual temperature transition than in regions around the necks of the latter and the resulting lower heat conduction flux leads to a higher maximum temperature $\Delta T_M + T_o$ in a beam with a uniform width. The $\Delta T_M + T_o$ for a beam with a nonuniform width can be calculated using $V_a = (I\rho/t)\int_0^L (dz/W(z))$ and (7)

$$\Delta T_M = \xi \frac{V_a^2}{8k\rho} \tag{11}$$

where

$$\xi \equiv \frac{4}{\left(1+e^{-\frac{L}{\beta}}\right)\left[\frac{1+e^{-\frac{L}{2\beta}}}{1-e^{-\frac{L}{2\beta}}}\int_0^{\frac{L}{\beta}}\sqrt{\frac{\left(e^{-x}+e^{x-\frac{L}{\beta}}\right)(1-e^{-x})\left(1-e^{x-\frac{L}{\beta}}\right)+8e^{-\frac{L}{\beta}}}{(1+e^{-x})^3\cdot\left(1+e^{x-\frac{L}{\beta}}\right)^3}}\,\mathrm{d}x\right]^2}.$$

Since $\Delta T_M = V_a^2/8k\rho$ for a beam with a uniform cross section, $\xi < 1$. It can be calculated for $L = 400\ \mu$m that $\xi \sim$ 0.77 for $\beta = 30\ \mu$m, ~0.82 for $\beta = 36\ \mu$m, and ~0.92 for $\beta =$ 45 μm. Consequently, ΔT_M at a given V_a for an actuator with uniform beams is generally larger than that with nonuniform beams; thus, a higher bound can be achieved for the η of the latter. In other words, beams with nonuniform widths are applicable to situations where a larger range of η is needed.

VI. Conclusion

Two design approaches to improve the performance of a chevron electrothermal in-plane actuator have been proposed. Their effectiveness is estimated analytically, verified using simulation, and demonstrated experimentally. Modification of the beam length and the tilt angle for an actuator of 49 beams exhibits an ~10% improvement in the performance figure-of-merit, defined to be the product of the actuation displacement and force, compared with that of the conventional structure. Furthermore, incorporating nonuniform beamwidth to produce a box-like high-temperature profile enhances the figure-of-merit by ~65% for β of 36 μm and L of 400 μm.

Acknowledgment

This work resulted from a course on the design of microsystems, jointly offered by The Hong Kong University of Science and Technology in Hong Kong and Kyoto University in Japan.

References

[1] K. Uchino, "Piezoelectric ultrasonic motors: Overview," *Smart Mater. Struct.*, vol. 7, no. 3, pp. 273–285, Jun. 1998.

[2] H. Guckel, J. Klein, T. Christenson, K. Skrobis, M. Laudon, and E. G. Lovell, "Thermo-magnetic metal flexure actuators," in *Tech. Dig.*

Solid-State Sens. Actuator Workshop, Hilton Head Island, SC, Jun. 1992, pp. 73–75.
[3] W. C. Tang, T.-C. H. Nguyen, and R. T. Howe, "Laterally driven polysilicon resonant microstructures," in *Proc. MEMS*, Feb. 1989, pp. 53–59.
[4] R. Legtenberg, J. Gilbert, S. D. Senturia, and M. Elwenspoek, "Electrostatic curved electrode actuators," *J. Microelectromech. Syst.*, vol. 6, no. 3, pp. 257–265, Sep. 1997.
[5] R. Hickey, M. Kujath, and T. Hubbard, "Heat transfer analysis and optimization of two-beam microelectromechanical thermal actuators," *J. Vac. Sci. Technol. A.*, vol. 20, no. 3, pp. 971–974, May/Jun. 2002.
[6] D. Yan, A. Khajepour, and R. Mansour, "Modeling of two-hot-arm horizontal thermal actuator," *J. Micromech. Microeng.*, vol. 13, no. 2, pp. 312–322, Mar. 2003.
[7] J. K. Luo, A. J. Flewitt, S. M. Spearing, N. A. Fleck, and W. I. Milne, "Three types of planar structure microspring electro-thermal actuators with insulating beam constraints," *J. Micromech. Microeng.*, vol. 15, no. 8, pp. 1527–1535, Aug. 2005.
[8] R. Cragun and L. L. Howell, "Linear thermomechanical microactuators," in *Proc. ASME Int. MEMS*, Nov. 1999, vol. 1, pp. 181–188.
[9] N. P. Konidaris, II, J. A. Kubby, and A. I. Sheinis, "Small solutions to the large telescope problem: A massively replicated MEMS spectrograph," in *Proc. SPIE*, Jul. 2008, vol. 7018, pp. 70182I–70181I-9.
[10] M. J. Sinclair, "A high force low area MEMS thermal actuator," in *Proc. Intersoc. Conf. Thermal Thermomech. Phenom. Electron. Syst.*, May 2000, pp. 127–132.
[11] J.-S. Park, L. L. Chu, A. D. Oliver, and Y. B. Gianchandani, "Bent-beam electrothermal actuators—Part II: Linear and rotary microengines," *J. Microelectromech. Syst.*, vol. 10, no. 2, pp. 255–262, Jun. 2001.
[12] J. K. Luo, A. J. Flewitt, S. M. Spearing, N. A. Fleck, and W. I. Milne, "Comparison of microtweezers based on three lateral thermal actuator configurations," *J. Micromech. Microeng.*, vol. 15, no. 6, pp. 1294–1302, Jun. 2005.
[13] P. J. Gilgunn, J. Liu, N. Sarkar, and G. K. Fedder, "CMOS-MEMS lateral electrothermal actuators," *J. Microelectromech. Syst.*, vol. 17, no. 1, pp. 103–114, Feb. 2008.
[14] L. Que, J.-S. Park, and Y. B. Gianchandani, "Bent-beam electro-thermal actuators for high force applications," in *Proc. IEEE Int. Conf. Micro Electro Mech. Sys.*, Jan. 1999, pp. 31–36.
[15] L. Que, J.-S. Park, and Y. B. Gianchandani, "Bent-beam electro-thermal actuators—Part I: Single beam and cascaded devices," *J. Microelectromech. Syst.*, vol. 10, no. 2, pp. 247–254, Jun. 2001.
[16] Y. Zhang, Q.-A. Huang, R.-G. Li, and W. Li, "Macro-modeling for polysilicon cascaded bent beam electrothermal microactuators," *Sens. Actuators A, Phys.*, vol. 128, no. 1, pp. 165–175, Mar. 2006.

Alex Man Ho Kwan (M'05–S'11) received the B.Eng.(Hons.) degree in electronic and communication engineering from the University of Hong Kong, Hong Kong, in 2003. From 2003 to 2005, he was with the Optical Communication Laboratory at The Hong Kong University of Science and Technology (HKUST), Kowloon, Hong Kong, where he worked on optoelectronic clock recovery techniques and received the M.Phil. degree. He is currently working toward the Ph.D. degree in electronic and computer engineering at HKUST.

From 2005 to 2009, he was an Engineer with SAE Magnetics (HK) Ltd., Hong Kong, where he focused on design of optoelectronic modules, reliability tests of vertical-cavity surface-emitting laser (VCSEL) diode packages, and product quality control of multi-chip front-end wireless modules on low temperature co-fired ceramic (LTCC) substrates. He is currently working in the Wireless Communication Laboratory, HKUST, under the supervision of Prof. K. J. Chen. His research interest is the design and implementation of GaN-based power electronics.

Sichao Song (S'11) was born in Tianjin, China, in February 1987. He received the B.S. degree in optoelectronics from Fudan University, Shanghai, China, in 2009. He is currently working toward the Ph.D. degree in electronic and computer engineering at The Hong Kong University of Science and Technology (HKUST), Hong Kong.

Since September 2009, he has been with the Wireless Communication Laboratory, HKUST, under the supervision of Prof. R. Murch. While there, he has focused on the design and implementation of reconfigurable antennas.

Xing Lu received the B.S. degree in microelectronics from Fudan University, Shanghai, China, in 2010. He is currently working toward the Ph.D. degree in electronic and computer engineering at The Hong Kong University of Science and Technology, Hong Kong.

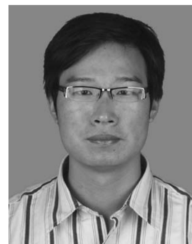

Lei Lu received the B.S. and M.S. degrees in microelectronics from Soochow University, Suzhou, Taiwan, in 2007 and 2010, respectively. He is currently working toward the Ph.D. degree in the Department of Electronic and Computer Engineering, The Hong Kong University of Science and Technology, Hong Kong.

Ying-Khai Teh (S'06) received the B.Eng.(Hons) degree in electronics and the M.Eng.Sc. degree from the Multimedia University, Cyberjaya, Malaysia, in 2005 and 2009, respectively. He is currently working toward the Ph.D. degree at The Hong Kong University of Science and Technology, Hong Kong, in the Integrated Power Electronics Laboratory.

His research interest is in energy harvesting circuit design.

Ying-Fei Teh received the B.Eng. degree in electronics from the Multimedia University, Cyberjaya, Malaysia, in 2009. He is currently working toward the M.Phil. degree at The Hong Kong University of Science and Technology, Hong Kong.

His research interest is network on chip.

Eddie Wing Cheung Chong received the B.Eng. and M.Phil. degrees in electronic and computer engineering from The Hong Kong University of Science and Technology, Hong Kong, in 2005 and 2007, respectively, where he is currently working toward the Ph.D. degree.

Yan Gao received the B.Eng. degree in optoelectronic science and technology from Huang Zhong University of Science and Technology, Wuhan, China, in 2009. She is currently working toward the Ph.D. degree at The Hong Kong University of Science and Technology, Hong Kong.

William Hau received the B.Eng. and M.Sc. degrees in mechanical engineering from The Hong Kong University of Science and Technology, Hong Kong, in 1999 and 2002, respectively, where he is currently working toward the Ph.D. degree in mechanical engineering.

His areas of research are printed electronics and ferroelectric memory for radio-frequency identifier (RFID) applications.

Mr. Hau is an associate member of the Institution of Mechanical Engineers. He is also a member of the Chinese Mechanical Engineering Society and the Institution of Engineers, Australia.

Fan Zeng received the B.Eng. degree from the Department of Precision Instruments and Mechanology, Tsinghua University, Beijing, China, in 2009. He is currently working toward the Ph.D. degree in the Department of Electronic and Computer Engineering, The Hong Kong University of Science and Technology, Hong Kong.

Man Wong (S'83–M'88–SM'00) was born in Beijing, China. From 1979 to 1984, he studied at the Massachusetts Institute of Technology, Cambridge, where he received the B.S. and M.S. degrees in electrical engineering.

From 1985 to 1988, he was with the Center for Integrated Systems, Stanford University, Stanford, CA, where he worked on tungsten-gate MOS technology and received the Ph.D. degree in electrical engineering. From 1988 to 1992, he was with the Semiconductor Process and Design Center, Texas Instruments Incorporated, Dallas, TX, and worked on the modeling and development of integrated-circuit metallization systems and dry/vapor surface-conditioning processes. He is currently with the Department of Electronic and Computer Engineering, The Hong Kong University of Science and Technology, Hong Kong. He was appointed as Honorary Guest Professors of Nankai University, Tianjin, China, in 2003, and Soochow University, Suzhou, China, in 2011. His research interests include microfabrication technology, device structure and material; physics and technology of thin-film transistors; organic light-emitting diode display technology; modeling and implementation of integrated microsystems; and thin-film solar cell device and process technology.

Dr. Wong is a member of Tau Beta Pi, Eta Kappa Nu, and Sigma Xi.

Chunmei Huang received the B.E. degree in mechanical engineering and automation from Jilin University, Changchun, China, in 2009. She is currently working toward the M.E. degree in The Department of Micro Engineering at Kyoto University, Kyoto, Japan.

Akira Taniyama received the B.E. degree in engineering science from Kyoto University, Kyoto, Japan, in 2010, where he is currently working toward the M.E. degree in The Department of Micro Engineering.

Yoshihide Makino received the B.E. degree in engineering science from Kyoto University, Kyoto, Japan, in 2010, where he is currently working toward the M.E. degree in The Department of Micro Engineering.

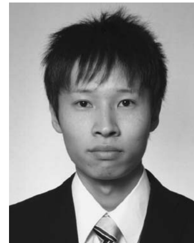

So Nishino received the B.E. degree in engineering science from Kyoto University, Kyoto, Japan, in 2010, where he is currently working toward the M.E. degree in The Department of Micro Engineering.

His research subject concerns gold nanoparticles and their application as nanotechnology devices.

Toshiyuki Tsuchiya (M'96) received the M.S. degree from the University of Tokyo, Tokyo, Japan, in 1993, and the Ph.D. degree from Nagoya University, Nagoya, Japan, in 2002.

He was with Toyota Central Research and Development Laboratories from 1993 to 2004. In 2004, he joined Kyoto University, Kyoto, Japan, as an Associate Professor, and he is currently with the Department of Micro Engineering of Kyoto University. He is currently engaged in the research of silicon surface micromachining, its application in microelectromechanical systems (MEMS), the mechanical property evaluation of micromaterials, and the reliability of MEMS devices.

Dr. Tsuchiya has been a member of the International Steering Committee of the IEEE MEMS conference since 2010, and he will cochair IEEE MEMS 2013 in Taipei, Taiwan. He is a member of the Materials Research Society, the Institute of Electrical Engineers of Japan, and the Japan Society of Mechanical Engineers.

Osamu Tabata (M'89–SM'01) was born in 1956. He received the M.S. and Ph.D. degrees from Nagoya Institute of Technology, Nagoya, Japan, in 1981 and 1993, respectively.

In 1981, he joined the Toyota Central Research and Development Laboratories, Inc., Aichi, Japan. In 1996, he joined the Department of Mechanical Engineering, Ritsumeikan University, Shiga, Japan. From September to December 2000, he was a Guest Professor at the Institute of Microsystem Technology, University of Freiburg, Germany, and from January to March 2001, he was a guest Professor at Eidgenössische Technische Hochschule Zürich, Zürich, Switzerland. In 2003, he joined the Department of Mechanical Engineering, Kyoto University, Kyoto, Japan. Since April 2005, he has been a Professor in the Department of Micro Engineering, Kyoto University. He is currently engaged in research on micro/nano processes, MEMS, and micro/nano system synthetic engineering. He has begun research to realize a unique and novel nanosystem by assembling the various functional components such as a microchip, a particle, a microcapsule, a cell, etc., with sizes ranging from nanometer to micrometer scale on a few-millimeter-square MEMS substrate. This technology is termed synthetic engineering for nanosystems (SENS), and experimental and theoretical research on the establishment of SENS is pursued.

Dr. Tabata has been a Senior Research Fellow at the Freiburg Institute for Advanced Studies since May 2010 and had a Visiting Professorship for Senior International Scientists of the Chinese Academy of Science in 2010. He is an Associate Editor of the JOURNAL OF MICROELECTROMECHANICAL SYSTEMS and an Editorial Board Member of *Sensors and Actuators*. Also, he is a program committee member of several international conferences. He was honored with the Science News Award for research on a "Monolithic pressure-flow sensor" in 1987, the Presentation Paper Award for research in "Anisotropic etching of silicon in tetramethylammonium hydroxide (TMAH) solutions" in 1992, the R&D 100 Award for research on "Thin film Young's modulus measurement apparatus" in 1993, and the R&D 100 Award for research on "Thin film tensile tester" in 1998, the Best Poster Award of the 19th Sensor Symposium on Sensors, Micromachines, and Applied Systems for "Determination of optimal mask movement pattern for moving mask deep X-ray lithography" in 2002, and the Best Patent Award from Ritsumeikan University for "Material processing and its apparatus using X-ray lithography" in 2004. He is a member of the Japan Society of Mechanical Engineers and the Japan Institute of Electronics Packaging and a senior member of the Institute of Electrical Engineers of Japan.